proceedings

Conference Proceedings Paper, The 4th International Electronic Conference on Atmospheric Sciences

Separation of Stratiform and Convective Rain Types using Data from an S-band Polarimetric Radar: A Case Study Comparing Two Different Methods†

Merhala Thurai [1,*], David Wolff [2], David Marks [2,3], Charanjit Pabla [2,3], and Viswanathan Bringi [1]

[1] Department of Electrical and Computer Engineering, Colorado State University, Fort Collins, CO 80523, USA; merhala@colostate.edu (M.T.); bringi@engr.colostate.edu (V.B.)
[2] NASA GSFC Wallops Flight Facility, Wallops Island, Virginia, USA; david.b.wolff@nasa.gov (D.W.), david.a.marks@nasa.gov (D.M.); charanjit.s.pabla@nasa.gov (C.P.)
[3] Science Systems and Applications, Inc., Lanham, MD, USA.
* Correspondence: merhala@colostate.edu; Tel.: +1-970-491-7678
† Presented at the 4th International Electronic Conference on Atmospheric Sciences, 16-31 July 2021, Online.

Abstract: Data from an S-band polarimetric radar located at a mid-latitude, coastal location are used to compare two different methods for identifying stratiform and convective rain regions. The first method entails the retrievals of two (main) parameters of the rain drop size distributions using the radar reflectivity and the differential reflectivity. The second technique is a well-known texture-based method which utilizes the radar reflectivity and its spatial variability. A widespread event with embedded line convection was used as a test case. The two methods were compared using 500m by 500m pixel resolution gridded data constructed from the radar volume scans. Only 12% of the pixels showed disagreement between the two methods.

Keywords: stratiform-convective rain separation; rain drop size distribution; S-band polarimetric radar.

Citation: Thurai, M.; Wolff, D.; Marks, D.; Pabla, C. Bringi, V. Separation of stratiform and convective rain types using data from an S-band polarimetric radar: A case study comparing two different methods. *Proceedings* **2021**, 65, x. https://doi.org/10.3390/xxxxx

Received: date
Accepted: date
Published: date

Publisher's Note: MDPI stays neutral with regard to jurisdictional claims in published maps and institutional affiliations.

1. Introduction

There are several different methods available in the literature to classify and separate stratiform and convective rain types. These include (a) the use of radar reflectivity 'texture' from weather radar scans, e.g. [1], (b) using ground in-situ measurements including surface disdrometers [2], [3], (c) using profiler observations, e.g. [4], and (d) based on the magnitude of up and downdrafts, e.g. [5]. Additionally, the estimated or retrieved characteristics of rain drop size distributions (DSD) have also been used to identify the two rain types [6], [7], and compared with the reflectivity-texture based method in [8], [9] using C-band radar observations in Darwin, Australia, which is a tropical region. In this paper, we perform similar comparisons between the same two methods (i.e. between the reflectivity texture-based method and the DSD-based method) but in the current study we utilize data from an S-band polarimetric radar (NPOL; e.g. [10]) at a mid-latitude coastal region, namely Wallops Island, Delmarva peninsula, USA.

In a very recent paper [11], the DSD-based separation method was tested using data from two collocated disdrometers based at the Wallops site. The two disdrometers were (i) a Meteorological Particle Spectrometer (MPS; [12]) which provided accurate measurements of drop concentrations for small and tiny drops (particularly for drop diameters below 1.2 mm), and (ii) a 2D video disdrometer (2DVD; [13], [14]) for drop concentrations above 1 mm. By combining both sets of measurements, the full DSD spectra were constructed and the rain-type classification was made using 1 and 3-minute DSDs. For each of these DSDs, the mass-weighted mean diameter, D_m and the normalized intercept parameter, N_W, were derived, and depending on where the each point lies in the N_W versus D_m domain, the corresponding rain type was determined. The classification was then 'visually' compared against RHI scans from the NPOL radar, made over the disdrometer site. Over 20 hours of 1 and 3 minute DSD data (and the corresponding RHI scans) were used for verification.

As a follow on, in this paper we examine the application of the same basic technique to the S-band NPOL radar data. An improved retrieval method is used to estimate N_W and D_m from the radar reflectivity and differential reflectivity measurements. Gridded data from -60 to +60 km along north-to-south and east-to-west are used at various altitudes from 1000 m to 3000 m above sea level, in steps of 500 meters. The (constant-altitude) gridded data were constructed from the NPOL radar volume scans taken during a relatively wide-spread event with embedded line convection which passed over the Wallops site on 30 April 2020. The lowest gridded level was used for pixel-by-pixel comparison against the reflectivity texture-based method from [1].

2. Estimating N_W and D_m from NPOL radar data

The equations used for retrieving (or estimating) N_W and D_m from the NPOL reflectivity and differential reflectivity (Z_h and Z_{dr} respectively) were previously given in [11] and hence is briefly described here. The estimation of D_m is a two step procedure, the first step involving the estimation of an intermediary parameter, D_m' which depends on two chosen reference moments [15]. If we denote these as Mi and Mj, then D_m' is given by:

$$\mathrm{D_m}' = \left(\frac{\mathrm{M_j}}{\mathrm{M_i}}\right)^{\frac{1}{(\mathrm{j-i})}} \quad (1)$$

At S-band, simulations have shown that D_m' can be directly estimated from Z_{dr} to within reasonable/acceptable accuracy. Fig. 1(a) shows the simulation points using 3-minute measured DSDs (i.e. full DSD spectra, but from two different locations, Huntsville, Alabama, which is a sub-tropical region, and Greeley, Colorado, which is a mid-latitude continental climate) as well as the fitted curve, given by:

$$\mathrm{D'_m} = 0.0822\ \mathrm{Z}_{dr}^3 - 0.4841\ \mathrm{Z}_{dr}^2 + 1.7515\ Z_{dr} + 0.628 \quad (2)$$

Next, we determine D_m from D_m'. Once again, S-band simulations have shown that this can be done to within good accuracy, as shown in panel (b) of Fig. 1. The fitted curve is given by:

$$D_m = 0.7977\ \mathrm{D'_m} + 0.0883 \quad (3)$$

Note both panels (a) and (b) show monotonic increase, hence no ambiguity will arise when using eq. (2) and (3).

The third and final step is to determine N_W. As shown in [11], N_W is given by:

$$\mathrm{N_W} = \left(\frac{4^4}{6}\right) \mathrm{N_0}' \quad (4)$$

where $$\mathrm{N_0}' = \mathrm{M_i}^{\frac{(\mathrm{j+1})}{(\mathrm{j-i})}}\ \mathrm{M_j}^{\frac{(\mathrm{i+1})}{(\mathrm{i-j})}} \quad (5)$$

To derive N_W, we need to make use of both the retrieved D_m as well as the radar reflectivity. Panel (c) shows the variation of $N_W/Z_{h\ (linear)}$ versus D_m where $Z_{h\ (linear)}$ is the radar reflectivity in linear units. The fitted curve (monotonic decrease) is given by:

$$\frac{\mathrm{N}_W}{Z_{h\,(linear)}} = 39.446\ {D'_m}^{-6.839} \quad (6)$$

In summary, equations (2), (3) and (6) are used to estimate N_W and D_m for each of the gridded pixels from the S-band scans.

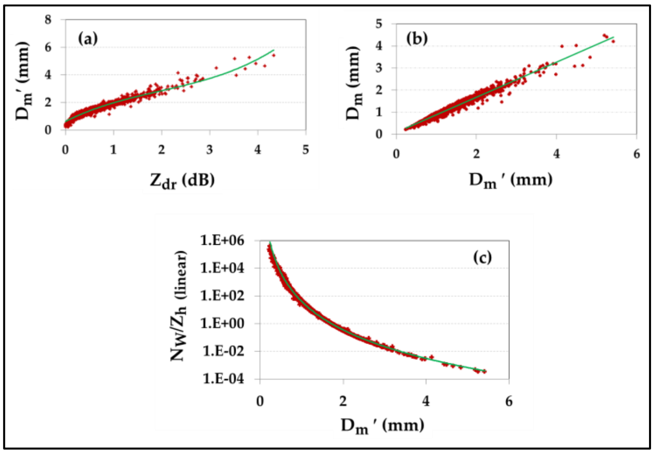

Figure 1. S-band simulation results of **(a)** D_m' versus Z_{dr}; **(b)** D_m with D_m'; **(c)** $N_W/Z_{h(linear)}$ versus D_m'.

3. NPOL data and the event on 30 April 2020

On 30 April 2020, a slow moving cold front passed over the WFF region. A NW/SE oriented line of strong convection with heavy rain moved through the region. Reflectivity within the line was as high as 60 dBZ in areas. The convective line was embedded in stratiform with reflectivity in the range 25 to 35 dBZ. As recorded in NASA rain gauges at Wallops, approximately 20 mm accumulated between 19 to 22 h UTC, the majority of which fell within 30 minutes associated with the convective line.

Figure 2(a) and 2(b) show the gridded data constructed from the volume scans taken at 21:05 UTC: (a) reflectivity and (b) differential reflectivity, both at 1000 m above sea level with a pixel resolution of 500m x 500m. The line convection shows reflectivities as high as 55 to 60 dBZ and differential reflectivities of > 2 dB in some regions. Note also, at azimuths of around 170 deg, some beam-blockage problems exist (which need to be omitted from the classification procedure).

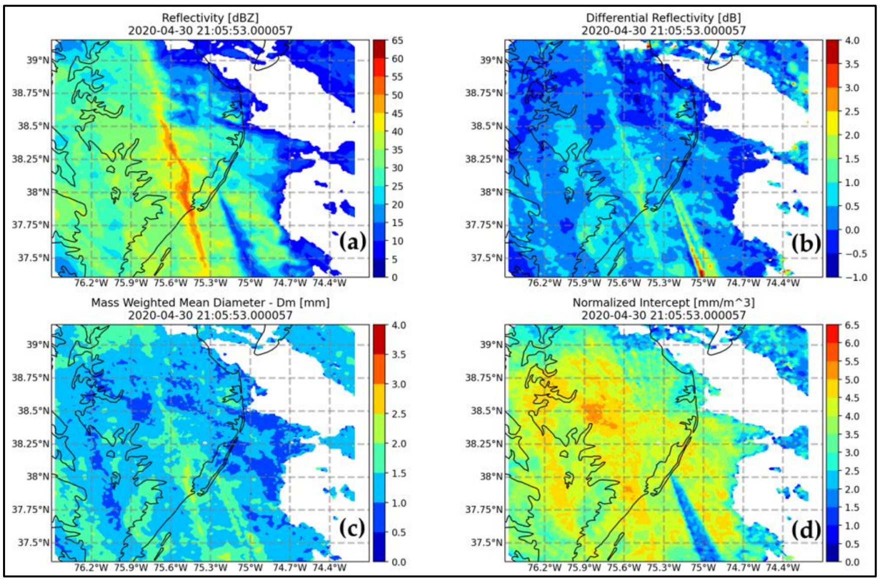

Figure 2. NPOL gridded data at 1000 m altitude with 500 m by 500 m pixel resolution; (a) Z_h; (b) Z_{dr}; (c) estimated D_m; (d) estimated N_W.

Panels (c) and (d) of Figure 2 show the estimated N_W and D_m, respectively, derived using eq. (2), (3) and (6). Once again, the effect of beam-blockage at ~170 deg azimuth is evident in the retrievals. Within the line convection itself, D_m values > 2 mm are seen in some regions.

4. Rain type classification

The gridded data ranging from -60 km to +60 km both in the North-South and the East-West directions were extracted and the classification based on the N_W -D_m values for each pixel was determined. As mentioned in [11], "a simple 'index' parameter, *i* (empirically-derived), was used to indicate whether the N_W versus D_m lie above or below the separation line". Value of *i* for each pixel is given by:

$$i = log_{10}(N_W^{est}) - log_{10}(N_W^{sep}) \quad (7)$$

where

$$log_{10}(N_W^{sep}) = c_1\, D_m^{est} + c_2 \quad (8)$$

In eq. (7), N_W^{est} is the estimated N_W for the specific pixel and D_m^{est} the (corresponding) estimated D_m. Note, in [11], equations (7) and (8) were applied to disdrometer-based DSD data. Note also that "values of c_1 and c_2 may vary somewhat depending on the location, but to be consistent with our previous study, they were set to −1.682 and 6.541, respectively". If, for a given pixel, *i* is negative, then it is categorized as stratiform rain and when *i* is positive it is categorized as convective rain. Additionally, we introduce another category, namely, 'Mixed' (or Uncertain/Transition), when the magnitude of *i* is less than 0.05, i.e. $-0.05 \le i \le 0.05$. Such a category was initially introduced in [16] based on measurements from large squall lines with trailing stratiform rain. The disdrometer measurements showed that they were able to identify the convective line and the stratiform rain areas quite easily but there was a transition region between the convective and the stratiform which showed a different Z-R than for pure convection versus pure stratiform. We use the term 'transition' here even if the storm type does not belong to the squall lines described in [16]. Based on the latter, a third category was introduced in [8], using the C-band CPOL radar data from Darwin, Australia (although in that study, a wider range for *i* was used, viz. $-0.1 \le i \le 0.1$). The third category has been termed transition, mixed or uncertain.

Panel (a) of Figure 3 shows the classification for the 1000 m altitude gridded data in Fig. 2. The orange/red color represents convective rain category, and the cyan/turquoise color for stratiform rain. The purple color represents the mixed category, which appears to be predominantly in regions surrounding convective rain areas. By comparison, panel (b) of Fig. 3 shows the texture-based classification from the texture-based method. Both plots show somewhat similar features, but to compare the classifications on a pixel-to-pixel basis, we show in panel (c) the matched/mismatched pixels. The colors represent the following:

Light blue/cyan:	when both methods classify as stratiform rain
Red:	when both methods classify as convective rain
Orange:	when DSD-based method classifies as convective rain and the texture method as stratiform rain
Green:	when DSD-based method classifies as stratiform rain and the texture method as convective rain
Purple:	when DSD-based method classifies as mixed type
Black:	when Z_{dr} is < 0 dB, which is omitted from the classification procedure.

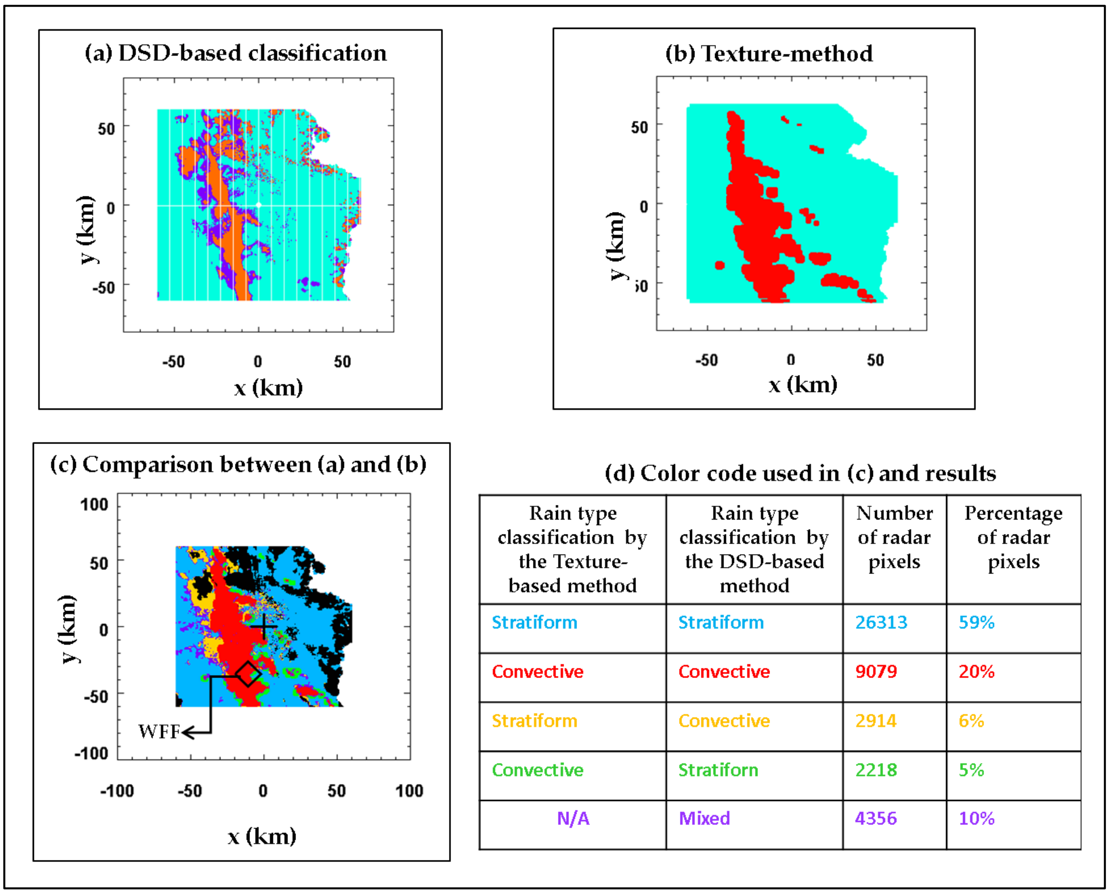

Rain type classification by the Texture-based method	Rain type classification by the DSD-based method	Number of radar pixels	Percentage of radar pixels
Stratiform	Stratiform	26313	59%
Convective	Convective	9079	20%
Stratiform	Convective	2914	6%
Convective	Straitforn	2218	5%
N/A	Mixed	4356	10%

Figure 3. (a) DSD-based rain type classification (orange: convective, cyan: stratiform, purple: mixed); (b) Texture-based classification (red: convective, cyan: stratiform); (c) matched and mismatched rain-types (see text for details); (d) table summarizing the number and percentages of matched and mismatched radar pixels (color-code used in (c).

In terms of percentage pixels, our comparison resulted in (a) 56% of the radar pixels being categorized as stratiform rain by both methods; (b) 21% as convective rain by both methods; and (c) a further 11% as the 'mixed' category from the DSD-based method. For the remaining 12% of the pixels, there was disagreement between the two methods which largely occurred in regions adjacent to (b).

A small but significant improvement was obtained when co-polar attenuation and differential attenuation were included in the radar-data correction procedures. Although at S-band the attenuation effects are largely negligible, it was found that for this particular case event, the differential propagation phase shift along certain azimuth angles (e.g. 220 deg) were sufficiently high to cause around 0.5 dB co-polar attenuation beyond the line convection. After applying the correction procedures, it was found that (a) 59% of the radar pixels were categorized as stratiform rain by both methods; (b) 20% as convective rain by both methods; and (c) a further 10% as the 'mixed' category from the DSD-based method. The percentage of 'mismatched' pixels reduced from 12% to 11%.

One of the main uses of the DSD-based separation technique is that it enables the ratios of the stratiform rain volume to convective rain volume to be determined from the gridded data. Such analysis is very important from the viewpoint of latent heat estimation since convective and stratiform rain have different heating rates. Further, since large scale numerical weather prediction models assume different ratios of convective to stratiform area and rain volume the retrieved products demonstrated here will form an important validation tool.

5. CFADs

Contoured Frequency-by-Altitude Diagrams (CFADs; [18]) are useful for examining vertical structures. For the Figure 2 case event, these were constructed separately for stratiform and convective rain regions (after applying the DSD-based separation), as well as for mixed precipitation. They are shown in Figure 4. The left panels show the reflectivity contours and the right panels show the differential reflectivity contours. One important aspect to note is that for convective rain (middle panels), both Z_h and Z_{dr} decrease from 3 down to 1 km, which in turn indicates that drop break-up is the dominant process [19]. On the other hand, for stratiform rain (top panels), Z_h is almost uniform from 3 to 1 km a.g.l. but Z_{dr} decreases, indicating, once again, the possible occurrence of drop break process but also indicating an increase in number concentration (per unit volume). These features were also observed in the stratiform rain regions of the outer rain-bands of Category-1 Hurricane Dorian (again over Wallops; [20]). A 1D MonteCarlo microphysical model using the super-particle concept (named McSnow; [21]) together with radiosonde data as model input also showed the importance of drop break-up even in light to moderate rain rates, being consistent with the radar observations [20].

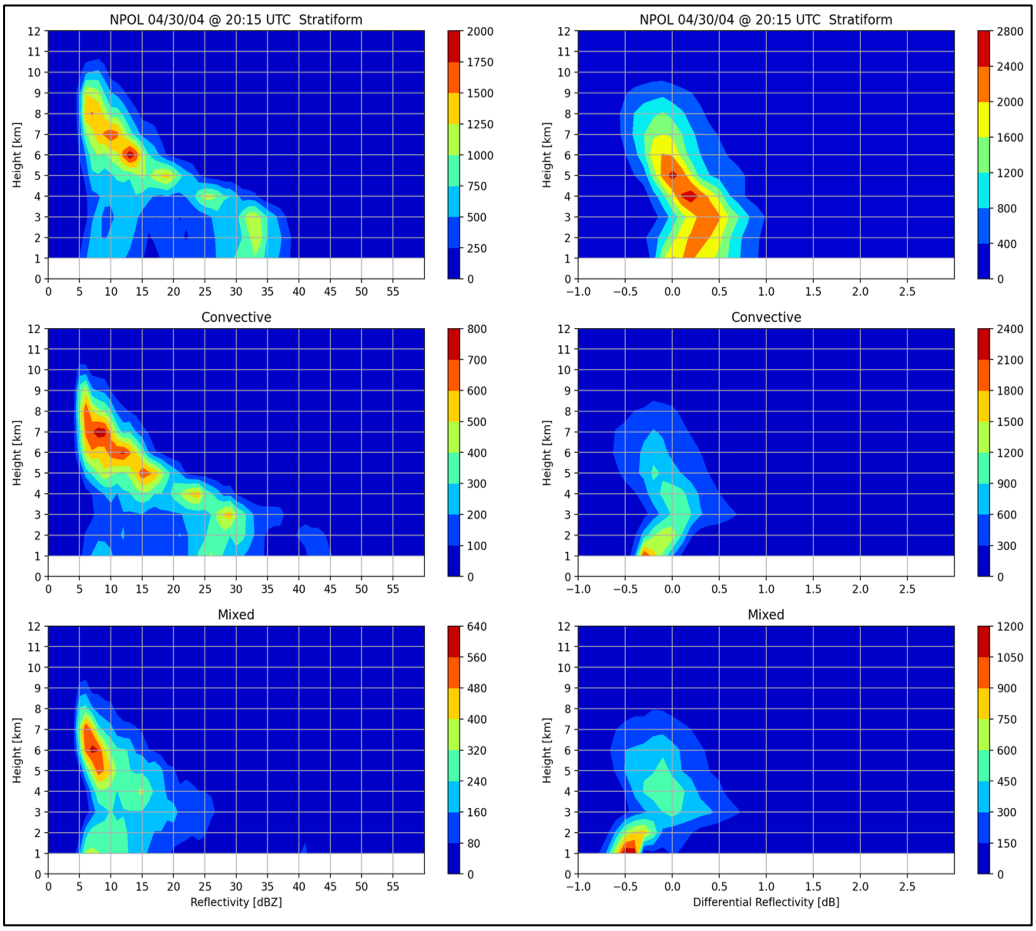

Figure 4. 2D histograms of Reflectivity (left panels) and Differential Reflectivity (right-panels) as a function of height [km], for stratiform rain (top panels), convective rain (middle panels) and mixed (bollom panels).

The corresponding CFADs for N_W and D_m are shown in Figure 5. The freezing height on this day was at around 3 km hence the retrieved N_W and D_m should be neglected above this height. In the rain region below, one main feature to be noted is that for both stratiform and convective rain, D_m decreases from 3 to 1 km but for the latter, the rate of decrease (with decreasing height) is noticeably higher, indicating that the break-up is more severe. For mixed precipitation, the rate of decrease is more similar to that for convective rain.

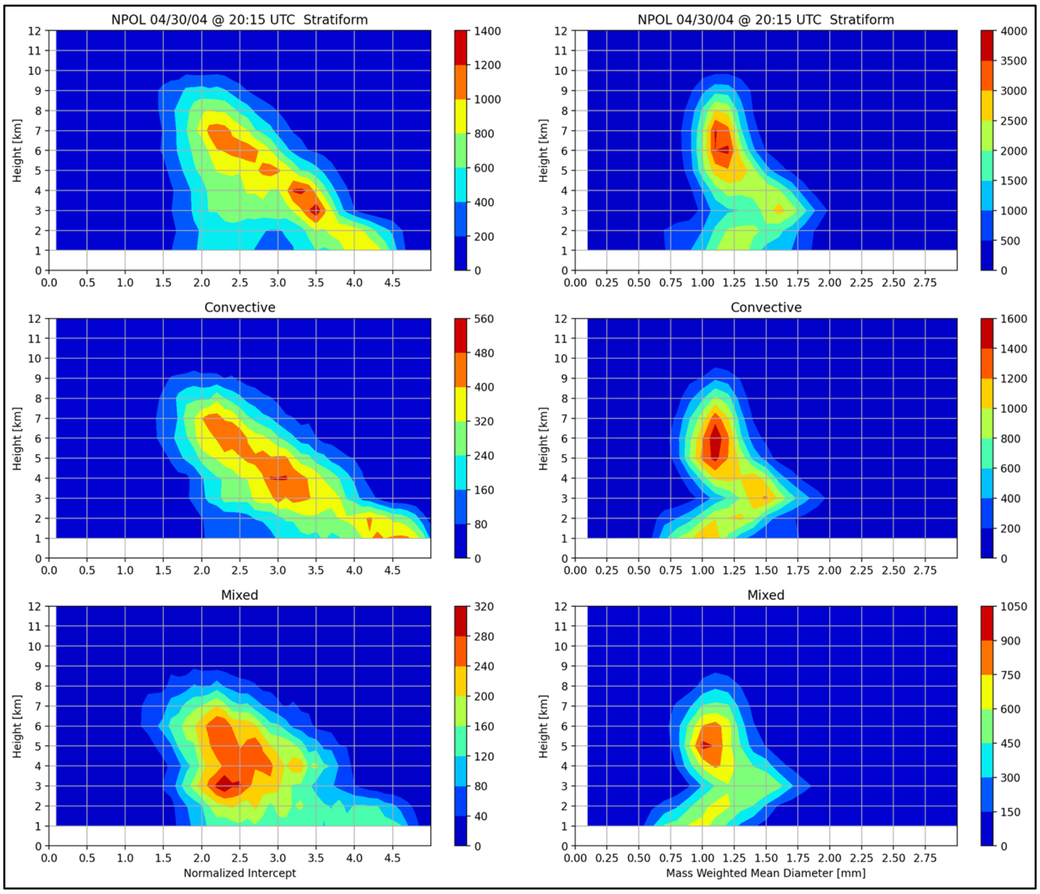

Figure 5. 2D histograms of N_W (left panels) and D_m (right-panels) as a function of height [km], for stratiform rain (top panels), convective rain (middle panels) and mixed (bollom panels).

6. Summary

The case study (of line convection embedded within a larger system) considered here has clearly shown that there is considerable agreement between the texture-based method in [1] and the DSD-based method in [6] and [8]. Only 12% of the gridded radar data pixels showed classification mismatch. When a simple attenuation-correction method (based on differential propagation phase shift) was applied to the S-band data, the percentage of mismatch reduced to 11%.

The DSD-based method utilized previously-derived retrievals for the two DSD parameters N_W and D_m. Stratiform and convective rain was based on where the N_W-D_m points lie in relation to the well-established separation line. Though the separation line was determined based on disdrometer data, we have shown that it can also be used for the gridded S-band NPOL radar data. A third category was also introduced to represent the mixed region. They tended to be in areas immediately surrounding the convective rain regions.

Contoured Frequency-by-Altitude Diagrams (CFADs) were also generated for the stratiform and convective rain separately. They indicate drop breakup to be a dominant process in the rain region below the freezing height. The rate of decrease (with decreasing height) of D_m was higher in the case of convective rain, implying that the drop breakup is more severe.

One caveat in the DSD-based technique is that there are a number of error sources which need to be considered when applying this technique. These include (i) radar measurement errors; (ii) retrieval algorithm errors (for example the 'scatter seen in Figure 1); and (iii) small uncertainties in the assumed separation line. Out of these, (i) is likely to be the most significant source of error. Nevertheless, from this case study, it seems likely that the DSD-based technique can be used for the S-band NPOL gridded data with reasonable accuracy. Further, it can be applied not just to the lowest gridded data but also to higher altitudes, i.e. up to the nominal freezing height.

Author Contributions: Conceptualization, M.T. and V. B. and D.W.; methodology, D.W. and M.T.; investigation, All Authors; resources, D.W.; data curation, D.M.; assistance, C.P.; writing—original draft preparation, M.T.; writing—review and editing, D.M. and V.B.; project administration, D.W.; funding acquisition, V.B. All authors have read and agreed to the published version of the manuscript.

Funding: This research was funded by NASA's Precipitation Measurement Mission via Grant Award Number 80NSSC19K0676.

Data Availability Statement: Data can be made available upon request to any of the authors.

Conflicts of Interest: The authors declare no conflict of interest. The funders had no role in the design of this study; in the collection, analyses, or interpretation of its data; in the writing of this manuscript, and in the decision to publish these results.

References

1. Steiner, M.; Houze, R.A.; Yuter, S.E. Climatological Characterization of Three-Dimensional Storm Structure from Operational Radar and Rain Gauge Data. *J. Appl. Meteor.* **1995**, *34*, 1978–2007.
2. Tokay, A.; Short, D.A. Evidence from Tropical Raindrop Spectra of the Origin of Rain from Stratiform versus Convective Clouds. *J. Appl. Meteor.* **1996**, *35*, 355–371.
3. Leary, C. A.; Houze, R. A., Jr. The Structure and Evolution of Convection in a Tropical Cloud Cluster, *Journal of Atmospheric Sciences*, **1979**, 36(3), 437-457.
4. Williams, C. R.; Ecklund, W. L.; Gage, K. S. Classification of precipitating clouds in the Tropics using 915-MHz wind profilers. *J. Atmos. Oceanic Technol.* **1995**, 12, 996–1012.
5. Atlas, D.; Ulbrich, C.W.; Marks, F.D., Jr.; Black, R.A.; Amitai, E.; Willis, P.T.; Samsur, C.E. Partitioning tropical oceanic convective and stratiform rains by draft strength. *J. Geophys. Res.* **2000**, 105, 2259-2267.
6. Bringi, V.N.; Williams, C.R.; Thurai, M.; May, P.T. Using dual-polarized radar and dual-frequency profiler for DSD characterization: A case study from Darwin, Australia. *J. Atmos. Oceanic Technol.* **2009**, *26*, 2107–2122.
7. Thurai, M.; Gatlin, P.N.; Bringi, V.N. Separating stratiform and convective rain types based on the drop size distribution characteristics using 2D video disdrometer data. *Atmos. Res.* **2016**, *169, Part B*, 416–423.
8. Thurai, M.; Bringi, V.N.; May, P.T. CPOL radar-derived drop size distribution statistics of stratiform and convective rain for two regimes in Darwin, Australia. *J. Atmos. Oceanic Technol.* **2010**, 27, 932-942.
9. Penide, G.; Kumar, V.; Protat, A.; May, P.T. Statistics of drop size distribution parameters and rain rates for stratiform and convective precipitation during the north Australian wet season. *Mon. Wea. Rev.* **2013**, 141, 3222-3237, doi:10.1175/MWR-D-12-00262.1.
10. Wolff, D.B.; Marks, D.A.; Petersen, W.A. General Application of the Relative Calibration Adjustment (RCA) Technique for Monitoring and Correcting Radar Reflectivity Calibration. *J. Atmos. Oceanic Technol.* **2015**, *32*, 496–506.
11. Thurai, M.; Bringi, V.; Wolff, D.; Marks, D.; Pabla, C. Testing the Drop-Size Distribution-Based Separation of Stratiform and Convective Rain Using Radar and Disdrometer Data from a Mid-Latitude Coastal Region. *Atmosphere* **2021**, 12, 392. https://doi.org/10.3390/atmos12030392
12. Baumgardner, D.; Kok, G.; Dawson, W.; O'Connor, D.; Newton, R. A new ground-based precipitation spectrometer: The Meteorological Particle Sensor (MPS). In Proceedings of the 11th Conf. on Cloud Physics, Ogden, UT, USA, Amer. Meteor. Soc. 3-7 June, **2002**, paper 8.6.
13. Schoenhuber, M.; Lammer, G.; Randeu, W.L. One decade of imaging precipitation measurement by 2D-video-distrometer. *Adv. Geosci.* **2007**, *10*, 85–90.
14. Schönhuber, M.; Lammer, G.; Randeu, W.L. The 2D-Video-Distrometer. In *Precipitation: Advances in Measurement, Estimation and Prediction;* Michaelides, S., Ed.; Springer: Berlin/Heidelberg, Germany, **2008**; pp. 3–31; ISBN 978-3-540-77654-3.
15. Lee, G.; Zawadzki, I.; Szyrmer, W.; Sempere-Torres, D.; Uijlenhoet, R. A General Approach to Double-Moment Normalization of Drop Size Distributions. *J. Appl. Meteor.* **2004**, *43*, 264–281.
16. Ulbrich, C. W.; Atlas, D. Radar Measurement of Rainfall with and without Polarimetry, *Journal of Applied Meteorology and Climatology* **2008**, 47(7), 1929-1939.
17. Tao, W.; Iguchi, T.; Lang, S. Expanding the Goddard CSH Algorithm for GPM: New Extratropical Retrievals. *J. Appl. Meteor. Climatol.* **2019**, *58*, 921–946.

18. Yuter, S. E., and Houze, R.A. 3-Dimensional kinematic and microphysical evolution of Florida cumulonimbus: 2. Frequency-distributions of vertical velocity, reflectivity, and differential reflectivity, ***Mon. Weather Rev.*** **1995**, 123, 1941 – 1963.
19. Carr, N.; Kirstetter, P. E.; Gourley, J. J.; Hong, Y. Polarimetric Signatures of Midlatitude Warm-Rain Precipitation Events, *Journal of Applied Meteorology and Climatology* **2017,** 56(3), 697-711.
20. Bringi, V.; Seifert, A.; Wu, W.; Thurai, M.; Huang, G.-J.; Siewert, C. Hurricane Dorian Outer Rain Band Observations and 1D Particle Model Simulations: A Case Study. *Atmosphere* **2020**, *11*, 879.
21. Brdar, S.; Seifert, A. McSnow: A monte-carlo particle model for riming and aggregation of ice particles in a multidimensional microphysical phase space. *J. Adv. Model. Earth Syst.* **2018**, 10, 187–206.